PCCP

Accepted Manuscript

ROYAL SOCIETY OF CHEMISTRY

www.rsc.org/pccp

Diversity of transition pathways in the course of crystallization into ice VII

Kenji Mochizuki, Kazuhiro Himoto, and Masakazu Matsumoto*

Department of Chemistry, Okayama University, 3-1-1 Tsushimanaka, Kitaku, Okayama 700-8530, Japan

Abstract

We report various types of pathways emerging in the course of freezing into a high pressure ice VII by large-scale molecular dynamics (MD) simulations at 10 GPa, 425 K. Some trajectories showed an apparently stepwise transition via the unique metastable "phase" in accordance with Ostwald's step rule. The metastable structure was identified as one of the tetrahedrally close-packed structures having the nature of a rotator phase (plastic phase). The unit cell consists of 21 water molecules that has not yet been reported by simulation or by experiments. Structure analysis of numerous trajectories reveals that the nucleation of ice VII easily occurs at the grain boundaries of the metastable embryos, known as epitaxy-mediated transformation in Ostwald's step rule. The size of the grain boundaries is thus responsible for the lifetime of the metastable phase. On the other hand, once the embryo of ice VII appears prior to that of the metastable phase in liquid, direct transition to ice VII takes place. We also show that the plastic behavior of the metastable phase is not uniform but is sensitive to the interaction strength to adjacent molecules and the local structure, thus we call "partially plastic ice".

Introduction

Homogeneous crystallization is a spectacular event in which molecules spontaneously acquire order by finding a specific intricate freezing pathway on the vast conformational space. It is of fundamental importance in both science and engineering.

The original idea of classical nucleation theory describes the direct nucleation of the thermodynamically most stable phase in supersaturated melts.[1,2]. In contrast, Ostwald empirically argued that an intermediate metastable phase could appear prior to the most stable phase to reduce the surface energy, which is known as Ostwald's step rule.[3] Since ten Wolde and Frenkel showed that the wetting layer can lower the free energy barrier in the crystallization of model globular proteins,[4] a metastable state/structure has been shown to play a key role in the nucleation of colloids,[5-8] protein solutions,[9] Lennard-Jones fluids,[10,11] and an inorganic component.[12]

Microscopically, on the other hand, the nucleation and growth of the crystal are controlled not only by the stability of the phases but also by the growth rate.[13] Cross-nucleation is another mode of the emergence of different phases in the crystallization process, in which the second crystal nucleates on the surface of the first crystal and grows. Note that these modes are related to each other and might happen simultaneously while one might only see the finally prevailed phase without any trace of the intermediate phases by experiments.[14] Direct observations by computer simulations of the nucleation and crystallization processes are therefore required.

Water is a network-forming substance and has a vast variety of polymorphs,[15-17] suggesting the possible diversity in metastable structures as well. In fact, the freezing of water at ambient pressure also indicates

that a metastable structure first emerges in liquid water or vapor.[18-20] Surface melting of ice is another example of the emergence of intermediate states.[21,22] Meanwhile, the melting of ice at ambient pressure occurs also in a stepwise molecular mechanism but in a different manner.[23]

There is another interesting aspect in high pressure ices. While the crystal structure of ice at low pressure is dominated by the hydrogen bond network structure and topology, their role reduces at higher pressure and packing becomes more substantial. In fact, each water molecule in ice VII, which is one of the densest ice phases, is coordinated by 8 adjacent water molecules at equidistances, but only four of them are hydrogen-bonded and the other four are sustained by a repulsive force.[16] Moreover, ice VII is predicted to become a plastic phase when heated, in which hydrogen bonds are transient and its structure is supported by repulsions.[24] The phase transition dynamics of the system possessing such competing interactions are intriguing and worth investigating.

In the present study, we performed a large number of isothermal-isobaric MD simulations to examine the spontaneous freezing into ice VII over numerous thermodynamic conditions on the temperature-pressure plane. Even at an identical condition (10 GPa, 425 K), various types of phase transitions were observed; some trajectories transformed into ice VII via a metastable phase by an epitaxy-mediated transformation using Ostwald's step rule,[14] while another found a direct pathway into ice VII. Detailed analyses of the structure-dynamics relationships and the pattern matching show that the unit cell of the metastable phase consists of 21 water molecules having heterogeneous rotativity, which is strongly correlated with the local structure.

Methods

We performed isothermal-isobaric MD simulations using GROMACS 4.5.5.[25] At a constant temperature, an equilibrium structure of liquid water at 1 GPa was pressurized to 5 GPa and was equilibrated for 500 ps. Several structures were then chosen from it and were instantaneously compressed to the target pressure by applying different momenta to obtain different trajectories. Two system sizes, N=3456 and N=15000, were considered, in which N is the number of water molecules in the simulation cell. Ten different MD simulations were performed for the smaller system at various thermodynamic conditions to survey where the phase transitions took place. Further simulations were performed at selected thermodynamic conditions with a larger system for detailed analyses. Temperature was controlled by a Nosé-Hoover thermostat.[26] Pressure was controlled by a Parrinello-Rahman barostat,[27] in which the rectangular simulation cell with a periodic boundary condition changes its shape anisotropically. The TIP5P rigid water model[28] is employed for the water-water intermolecular potential function. The Lennard-Jones interaction term of the intermolecular potential function is truncated at 9.0 Å without any dispersion corrections; the Coulombic term is also truncated at 9.0 Å with the Particle-Mesh Ewald technique[29] for its long-range correction. The time step of MD is 2 fs and the simulation time is 5 ns for every MD unless the formation of ice VII is completed.

Results and Discussion

Figure 1 indicates the pressure-temperature conditions where MD simulations were performed for the system of N=3456. Phase boundaries for the present water model were determined in previous computational studies.[30,31] More than 10 different trajectories were examined at each thermodynamic condition. Three different cases were found: (a) some trajectories exhibited stepwise crystallization into ice VII

from liquid water via an intermediate state; (b) liquid water directly transformed into ice VII for all the trajectories; (c) no phase transition occurred within 5 ns.

Here, we focus on the phase transitions at 10 GPa, 425 K (case (a)), in which the largest number of trajectories exhibited stepwise phase transitions. We then performed additional 39 MD simulations under the thermodynamic condition with a larger number of molecules, N=15000. All of them transformed from liquid water within 5 ns to ice VII or an intermediate state. Of 39 trajectories, 25 crystallized directly to ice VII, and five showed the emergence of an intermediate state persisting even up to 5 ns, while nine show stepwise crystallization to ice VII via an intermediate state. Thus, more than one third of MD trajectories exhibited the intermediate state prior to crystallization to ice VII.

Figure 2(a) shows the time evolution of enthalpies of three typical trajectories, named I, II, and III. In trajectory I, three distinct stages were clearly observed. According to the geometrical analysis mentioned later, the initial and final stages were identified as the liquid state and ice VII, respectively. After a waiting period of 550 ps in the liquid state, the system started to transform into the intermediate state between liquid and ice VII. In this trajectory, two different nuclei formed almost simultaneously, as shown later. Two thermodynamic conditions (425 K, 10 GPa) were observed deep inside the region of ice VII and possibly outside the spinodal lines of the liquid-VII phase boundary. Multiple nucleation of the intermediate state is thus regarded as a consequence of spinodal decomposition,[32] which also accounts for the fact that the intermediate state always nucleates after a similar induction period, about 700 ps, after compression. The intermediate state persists for 510 ps with a gradual decrease in enthalpy and finally ice VII nucleates at 1060 ps. Note that positive average enthalpy indicates that the repulsion is dominant in molecular interactions.

No transformation from ice VII to the intermediate state was observed in any trajectory. This intermediate state should therefore be a metastable state that appears in the crystallization process to ice VII, a phenomenon that is in agreement with Ostwald's step rule. One can see in trajectory III that the intermediate metastable state persisted for a long time, suggesting that there is a free energy barrier between the metastable state and ice VII. Note that even extra 15 ns for the trajectory III did not turn it to ice VII.

In order to elucidate the averaged dynamic aspects of the metastable state, we calculated the mean square displacement (abbreviated as MSD) $\langle|\mathbf{r}_i(t) - \mathbf{r}_i(0)|^2\rangle$ and the reorientational correlation function (RCF) $\langle\mathbf{u}_i(0)\cdot\mathbf{u}_i(t)\rangle$, where $\mathbf{r}_i(t)$ and $\mathbf{u}_i(t)$ are the center-of-mass position and the unit vector along the dipole direction, respectively, of molecule i at time t; the bracket $\langle...\rangle$ denotes the ensemble average. Figure 2(b) shows MSD while (c) RCF for the short periods of the liquid state (period A; 300-400 ps), metastable state (B; 850-950 ps), and ice VII (C; 2500-2600 ps) regarding trajectory B. The slope of MSD, which is a measure of diffusivity, is nearly zero at B and C, indicating that the translational motions are limited to vibrations around the lattice sites. Meanwhile, the RCF of period B decays as that of period A. These dynamic characteristics indicate that each water molecule rotates at the lattice point like a plastic phase,[33] however, its structure is quite different from already reported bcc or fcc plastic ice phases.[30,34]

In plastic ice, the packing of molecules outweighs the HB in determining the lattice form. We therefore focused on the arrangement of oxygen atoms to identify the packing structure.

Two water molecules are regarded to be adjacent when the oxygen atoms of both water molecules are closer than 3.8 Å, which is carefully chosen so as to contain second neighbors in the bcc lattice of ice VII but not to contain second neighbors in the fcc lattice. A triplet and a quartet of mutually adjacent molecules make up a triangle and a tetrahedron, respectively, and the tetrahedral arrangement indicates a higher-order structure in this unknown metastable crystal. Figure 3(a) shows typical arrangements; a tetragonal bipyramid composed of four face-sharing tetrahedra, which is a typical building block of a bcc lattice, and a pentagonal bipyramid composed of five face-sharing tetrahedra, which is a typical building block of the Frank-Kasper[35,36] and Laves phases.[37-39] Hexagonal bipyramids exist in both lattice structures. Note that a tetragonal bipyramid is not a regular but an oblate octahedron in which two apexes are also regarded as being adjacent to each other, according to our criterion. An fcc lattice consists of regular octahedra and tetrahedra with a fixed appearance ratio of 1:2, and are clearly distinguishable by this structure analysis. The present structure is filled mostly by tetrahedra. Regular octahedra made up only 7.5% of tetrahedra and therefore it is different from an fcc lattice. In general, such a structure is termed a tetrahedrally close-packed structure.[35,36,40]

Figure 3(b) shows the time evolution of the number of tetragonal and pentagonal bipyramids per water molecule, denoted as N_4 and N_5, along trajectories I and II. In trajectory I, N_5 increases sharply when liquid transforms into the metastable state, while N_4 decreases. Then, N_4 increases when the metastable state transforms into ice VII, while N_5 decreases. Eventually they vanish. Changes in the number of both bipyramids observed in trajectory II are similar to those at the first step in trajectory I.

The trajectories are mapped against density and N_4 in Figure 3(c), which indicates that trajectories I and II follow the same path to the metastable state, while trajectory III goes directly to ice VII. The other 36 MD trajectories obtained under the same condition are also mapped in a light color. There obviously exist many different pathways owing to the metastable state.

A crystal involves periodicity. Pattern matching is a powerful technique that can detect the periodic appearance of local patterns in an unknown structure. In the present study, a local molecular arrangement within 8 Å around an arbitrarily chosen water molecule was used as a template, and similar molecular arrangements were sought among the simulation cell. By translating and rotating the template, dozens of optimal arrangements, i.e. arrangements of highest similarity, for a template to match the molecular positions in the simulation cell, were found. Similarity was measured by the sum square displacement of molecules between the template and the closest molecule in the simulation cell. Practically, the similarity measure between local structures around molecules i and j is defined as the minimal value of

$$s(i,j;\mathbf{R},l) = \sum_{k\in U_i} \left|\mathbf{r}_{ik} - \mathbf{R}\mathbf{r}_{jl(k)}\right|^2$$

by optimizing the choice of a rotation matrix $\mathbf{R}$ and a one-to-one mapping $l(k)$ from molecule k to a molecule near molecule j, where $\mathbf{r}_{ik} \equiv \mathbf{r}_k - \mathbf{r}_i$ is a relative vector from molecule i to k, U_i denotes a set of molecules in the 8 Å neighborhood of molecule i, and molecular orientation is ignored. The matched structures are then averaged to obtain the minimal unit of repetition, i.e. the unit cell.

Pattern matching was performed for the molecular arrangements at 5000 ps of trajectory II to obtain the unit cell, and it was confirmed that the same unit cell also matched other trajectories in the metastable state. The unit cell is approximately rhombohedral ($a \simeq 7.1$ Å) and all angles (α, β, γ) are almost 90 degrees.

Figure 4(a) and 4(b) shows the smallest unit cell. The number of water molecules in the unit cell (Z) is 21, which is the second largest after ice V (Z = 28) among water polymorphs. Note that the unit cell was estimated from a limited number of samples by computer simulation and therefore involves inaccuracy. Although our survey of the unit cell also suggests a possible superstructure with a larger periodicity, it could be an artifact influenced by the finite size effect of the simulation box. We therefore regard the unit structure of Z=21 as the unit cell of the metastable crystal in the present study.

The rhombohedral cell with Z=21 is uncommon. Some other phases have been reported: phase Ib of CCl_4 with α=90° and phase II of $(CH_3)_3CBr$ with α=89.19°.[41] However, the molecular arrangements in these unit cells remains unknown.

The unit cells of the metastable phase and ice VII detected in trajectory I (300 ps, 580 ps, 760 ps, 1130 ps, and 1900 ps) are shown in Figure 5(a) to visualize the two phase transitions via nucleations. Figure 5(b) shows the total number of local structures that loosely matched (s < 10.0 Å^2) with the unit cell of the metastable phase (green line) and strictly matched (s < 2.0 Å^2) the eightfold unit cell of ice VII (blue line), which are represented by the cubes and blue dots in Fig. 5(a), respectively. Interestingly, two nuclei appear at the first nucleation of the metastable phase, as was already mentioned in the previous section. Both nuclei start growing but the larger one gradually digests the smaller one in order to decrease the area of the grain boundary, known as Ostwald ripening, which also accompanies a gradual decrease in enthalpy. Movies for trajectories I, II, and III are found in the Supplementary Information.

All 39 different MD trajectories became frozen within 5 ns. As was already mentioned, the initial nuclei always emerged after a similar induction period, around 700 ps on average, ice VII in 25 trajectories and the metastable phase in 14 trajectories. Nine out of the latter trajectories re-transformed into ice VII via another nucleation. The occurrence and rate of the second transition was found to be strongly dependent on the microscopic structure.

In general, when the initial nucleus has the structure of ice VII, it grows rapidly and turns the whole system into an almost perfect single crystal of ice VII within 200 ps after nucleation (trajectory II). On the other hand, the initial nucleus of the metastable phase tends to accompany the formation of the grain boundaries, probably because of the deeply supersaturated thermodynamic condition and of its giant unit cell. Note that even a single crystal may form the grain boundary with itself because of the periodic boundary condition applied in the computer simulation.

There are some typical cases in the nucleation of the metastable phase. Nine trajectories yielded a single nucleus of the metastable phase, five of which evolved to a single crystal of the metastable phase without a grain boundary and no further transition to ice VII was observed (trajectory III). The four other trajectories accompanied the grain boundary to itself and ice VII nucleated at the boundary, but the crystal growth of ice VII was found to be very slow in these cases.

Simultaneous double nucleations were observed in five trajectories. Both nuclei initially grew rapidly but the larger nucleus slowly digested the smaller one at a later stage in order to reduce the interface area. The broad grain boundaries between them allowed the rapid nucleation of ice VII (trajectory I). Thus the second transition to ice VII proceeded fastest in this case. The direction of one of the crystal axes of ice VII was always common with that of the metastable phase, suggesting that the nucleus of ice VII emerges via an epitaxy-mediated transformation.[14]

A recent study observed the cross-nucleation of clathrate hydrates, i.e. nucleation and growth of a second crystal on the surface of a first crystal.[13] Although ice VII actually emerges heterogeneously on the boundary of the metastable crystal grains in stepwise transitions, the stable phase finally digests the metastable phase. This is probably because the metastable phase in the present study was much less stable than the stable phase, and also since the metastable phase is not a solid crystal but a "plastic", i.e. mechanically soft phase.

To confirm the results, we have performed additional MD simulations using TIP4P/2005 water model[42] with the same treatment of the long range interaction as mentioned in the method section. The stepwise phase transition via the same metastable phase is also observed, as shown in Figures S1 of Supplementary Information.

Next, we revealed the heterogeneous rotation dynamics in the metastable phase by analyzing the correlation between the local structure, local density, number of HBs and the inclination to rotate.

The local structure around a water molecule is characterized by the number of tetragonal (n_4) and pentagonal bipyramids (n_5) that contain the molecule as an apex. Colors in Figure 4(a) represent n_4 values in the ideal unit cell of the metastable phase, which varies from place to place. Note that all water molecules in the ideal ice VII have uniform values of $n_4 = 6$ and $n_5 = 0$. In general, n_4 was inversely correlated with n_5 in both solid structures.

We then examine the oxygen–oxygen radial distribution functions (RDFs), $g_{OO}(r)$, to elucidate how the local density distribution was related to the local structure. $g_{OO}(r)$ in Figure 6(a) are plotted for water molecules in three different environments; those with $n_4 = 0$ and 6 in the metastable phase and all molecules in ice VII, which are sampled from 10 frames between 4900 and 5000 ps of trajectory II and III, respectively.

Two notable features were found: (1) the $g_{OO}(r)$ of $n_4 = 0$ and $n_4 = 6$ are very different. The first peak of the $g_{OO}(r)$ of $n_4 = 6$ resides is closer and has a broader shoulder than that of $n_4 = 0$. (2) The first peak of the $g_{OO}(r)$ of $n_4 = 6$ resides are closer than that of ice VII, suggesting that the local density around a water molecule with $n_4 = 6$ in the metastable phase is higher than that in ice VII despite the fact that the average density of the metastable phase is lower than that of ice VII.

The ratio of water molecules having four HBs with their neighbors is plotted against n_4 in Figure 6(b), which was calculated by using 10 frames between 4900 and 5000 ps of trajectory II. Here two water molecules were considered to be hydrogen-bonded if their intermolecular hydrogen-oxygen distance was shorter than 2.1 Å, which was determined by the location of the first minimum of the hydrogen-oxygen RDF. The magnitude of rotational motion of a water molecule was evaluated by the rotation angle between two orientations at instants t and t+10 ps and its average value was also plotted against n_4 in Figure 6(b), which was also calculated using 10 frames between 4900 and 5000 ps of trajectory II.

These results indicate that a water molecule with larger n_4 tends to have a higher local density, forming four HBs, and exhibits less facile rotation.

This can be explained from a viewpoint of energy landscape and coordination number. In general, larger coordination number for a water molecule yields a smoother energy landscape for rotation. (Remember, the strongest structure for ice is four-coordinated!) Moreover, larger n_5 (smaller n_4) in a local structure suggests a more isotropic (icosahedral) coordination space around a water molecule, which is indicated by the first sharp peak in RDF for $n_4 = 0$ in Fig 6(a).

The broad first-neighbor peak of $n_4 = 6$ in Fig 6(a), on the other hand, suggests the non-uniform coordination of the first neighbor molecules. Some of the neighbor molecules are closer in larger n_4 than in smaller n_4, which in turn tightens the hydrogen bonding to neighbor molecules.

Thus, the metastable phase, say "*partially plastic ice*", is shown to have heterogeneous rotativity, reflecting the local structure around a water molecule.

Such heterogeneity in rotativity in a crystal is also found in Phase II of CH_4 [43] and in the one-dimensional plastic phase of SF_6.[44] In these crystals, geometric frustration induces heterogeneity. In the case of partially plastic ice, on the other hand, competition between the geometrical (packing) characteristic and preference of making four HBs yields the heterogeneous dynamics.

Summary

In summary, MD simulations present spontaneous crystallization to ice VII from liquid water along various pathways. The majority is direct transformation but there are many other paths via an intermediate metastable phase in accordance with an epitaxy-mediated transformation in Ostwald's step rule. The structure-dynamics relationship suggests that the lattice structure of the metastable phase is governed by the packing effect as well as by HB stabilization. The water molecules are orientationally disordered, and interestingly the plastic behavior is not uniform but is sensitive to the local structure around a water molecule.

It is interesting to know how the system spontaneously and quickly finds such an intricate and large (Z=21) structure prior to a much simpler bcc structure (Z=2), and how the molecules recognize and adjust their proper location to acquire a long range order of the crystal with such a large unit cell.

It is worthwhile to compare the significant differences between partially plastic ice and already reported plastic ices. bcc and fcc plastic ices are regarded as derivatives from ice VII, because bcc plastic ice has the same lattice structure as ice VII and can be transformed into fcc plastic via a Martensitic phase transition with local molecular displacements.[34] In contrast, the lattice arrangement of partially plastic ice is different from any other ice structure. This fact suggests that plastic ice is not forced to resemble any conventional ice structure satisfying an ice-rule.

There is a wide variety of tetrahedrally close-packed structures represented by Frank-Kasper and Laves phases. It is therefore reasonable to consider that various types of metastable plastic ices have yet to be discovered under high pressure.

Supporting Information

Movies of trajectory I, II, and III, colored in the same manner of Fig.5(a).

Corresponding Author

vitroid@gmail.com

Notes

The authors declare no competing financial interest.

Acknowledgement

Most of the calculations were carried out at the Research Center for Computational Science of NINS, Okazaki, Japan. The authors thank Dr. T. Yagasaki for meaningful discussions. KH thanks Japan Society for the Promotion of Science (JSPS) for its support by *Research Fellowship for Young Scientist.*

References

(1) Oxtoby, D. W. *J. Phys.-Condes. Matter* 1992, *4*, 7627.
(2) Oxtoby, D. W. *Accounts Chem. Res.* 1998, *31*, 91.
(3) Ostwald, W. *Z. Phys. Chem.* 1897, *22*, 289.
(4) tenWolde, P. R.; Frenkel, D. *Science* 1997, *277*, 1975.
(5) Auer, S.; Frenkel, D. *Nature* 2001, *409*, 1020.
(6) Anderson, V. J.; Lekkerkerker, H. N. W. *Nature* 2002, *416*, 811.
(7) Sanz, E.; Valeriani, C.; Frenkel, D.; Dijkstra, M. *Phys. Rev. Lett.* 2007, *99*, 055501.
(8) Zhang, T. H.; Liu, X. Y. *J. Phys. Chem. B* 2007, *111*, 14001.
(9) Vekilov, P. G. *Cryst. Growth Des.* 2004, *4*, 671.
(10) Anwar, J.; Boateng, P. K. *J. Am. Chem. Soc.* 1998, *120*, 9600.
(11) Lutsko, J. F.; Nicolis, G. *Phys. Rev. Lett.* 2006, *96*, 046102.
(12) Chung, S. Y.; Kim, Y. M.; Kim, J. G.; Kim, Y. J. *Nat. Phys.* 2009, *5*, 68.
(13) Nguyen, A. H.; Molinero, V. *J. Chem. Phys.* 2014, *140*, 084506.
(14) Niekawa, N.; Kitamura, M. *Crystengcomm* 2013, *15*, 6932.
(15) Eisenberg, D.; Kauzmann, W. *The Structure and Properties of Water*; Oxford University Press, 1969.
(16) Petrenko, V. F.; Whitworth, R. W. *Physics of Ice*; Clarendon Press, 1999.
(17) Salzmann, C. G.; Radaelli, P. G.; Slater, B.; Finney, J. L. *Phys. Chem. Chem. Phys.* 2011, *13*, 18468.
(18) Matsumoto, M.; Saito, S.; Ohmine, I. *Nature* 2002, *416*, 409.
(19) Malkin, T. L.; Murray, B. J.; Brukhno, A. V.; Anwar, J.; Salzmann, C. G. *Proc. Natl. Acad. Sci. U. S. A.* 2012, *109*, 1041.
(20) Murray, B. J.; Knopf, D. A.; Bertram, A. K. *Nature* 2005, *434*, 202.
(21) Faraday, M. *Experimental Researches in Chemistry and Physics*; R. Taylor and W. Francis, 1859.
(22) Sazaki, G.; Zepeda, S.; Nakatsubo, S.; Yokoyama, E.; Furukawa, Y. *Proc. Natl. Acad. Sci. U. S. A.* 2010, *107*, 19702.
(23) Mochizuki, K.; Matsumoto, M.; Ohmine, I. *Nature* 2013, *498*, 350.
(24) Himoto, K.; Matsumoto, M.; Tanaka, H. *Phys. Chem. Chem. Phys.* 2011, *13*, 19876.
(25) Hess, B.; Kutzner, C.; van der Spoel, D.; Lindahl, E. *J. Chem. Theory Comput.* 2008, *4*, 435.
(26) Nose, S. *J. Chem. Phys.* 1984, *81*, 511.
(27) Parrinello, M.; Rahman, A. *J. Appl. Phys.* 1981, *52*, 7182.
(28) Mahoney, M. W.; Jorgensen, W. L. *J. Chem. Phys.* 2000, *112*, 8910.
(29) Darden, T.; York, D.; Pedersen, L. *J. Chem. Phys.* 1993, *98*, 10089.
(30) Takii, Y.; Koga, K.; Tanaka, H. *J. Chem. Phys.* 2008, *128*, 204501.
(31) Himoto, K.; Matsumoto, M.; Tanaka, H. *Phys. Chem. Chem. Phys.* 2014, *16*, 5081.
(32) Bhimalapuram, P.; Chakrabarty, S.; Bagchi, B. *Phys. Rev. Lett.* 2007, *98*.
(33) Parsonage, N. G.; Staveley, L. A. K. *Disorder in Crystals*; Clarendon Press, 1978.
(34) Aragones, J. L.; Vega, C. *J. Chem. Phys.* 2009, *130*.
(35) Frank, F. C.; Kasper, J. S. *Acta Crystallographica* 1958, *11*, 184.
(36) Frank, F. C.; Kasper, J. S. *Acta Crystallographica* 1959, *12*, 483.
(37) Laves, F.; Witte, H. *Metallwirtschaft* 1935, *14*, 645.
(38) Laves, F. *Naturwissenschaften* 1939, *27*, 65.
(39) Friauf, J. B. *J. Am. Chem. Soc.* 1927, *49*, 3107.
(40) Shoemaker, D. P.; Shoemaker, C. B. *Acta Crystallogr. Sect. B-Struct. Commun.* 1986, *42*, 3.
(41) Barrio, M.; Pardo, L. C.; Tamarit, J. L.; Negrier, P.; Salud, J.; Lopez, D. O.; Mondieig, D. *J. Phys. Chem. B* 2006, *110*, 12096.
(42) Abascal, J. L. F.; Vega, C. *J. Chem. Phys.* 2005, *123*, 234505.
(43) Nakahata, I.; Matsui, N.; Akahama, Y.; Kawamura, H. *Chem. Phys. Lett.* 1999, *302*, 359.
(44) Pawley, G. S.; Dove, M. T. *Chem. Phys. Lett.* 1983, *99*, 45.

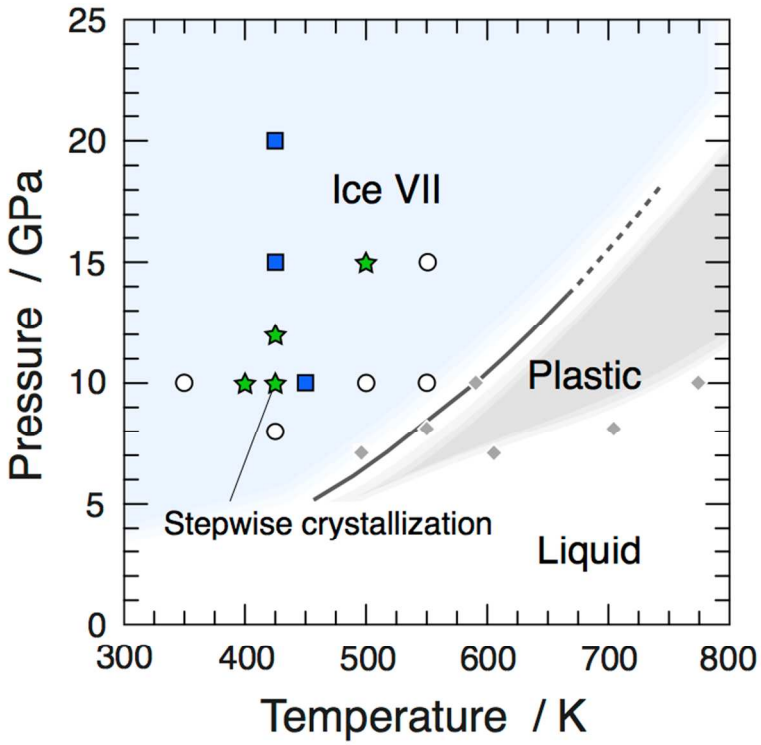

Figure 1. Phase diagram of water proposed previously and the locations where we performed MD simulations in this study. Coexistence and critical lines between ice VII and bcc plastic ice by Himoto *et al*.[31] are plotted with solid and dashed lines, respectively. Phase boundaries between ice VII and bcc plastic ice, bcc plastic ice and liquid water by Takii *et al.* [30] are indicated by gray diamonds. Blue squares indicate only direct transitions to ice, white circles show no phase transition within 5 ns while green stars indicate both direct and stepwise transitions.

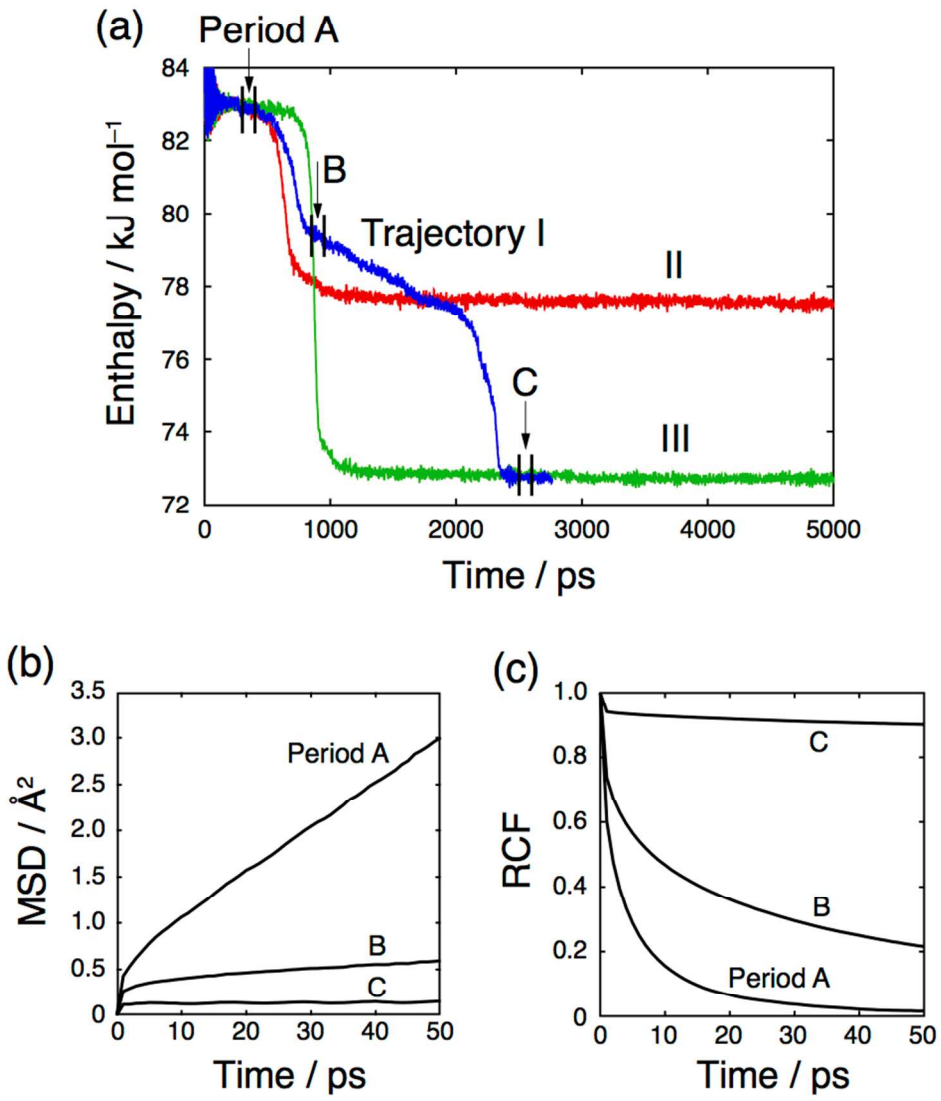

Figure 2. (a) Time evolution of enthalpies of three typical trajectories I (blue), II (red), and III (green). (b) Mean square displacement (MSD) and (c) reorientational correlation function (RCF) for the liquid state (period A), metastable state (B), and ice VII (C) in trajectory I.

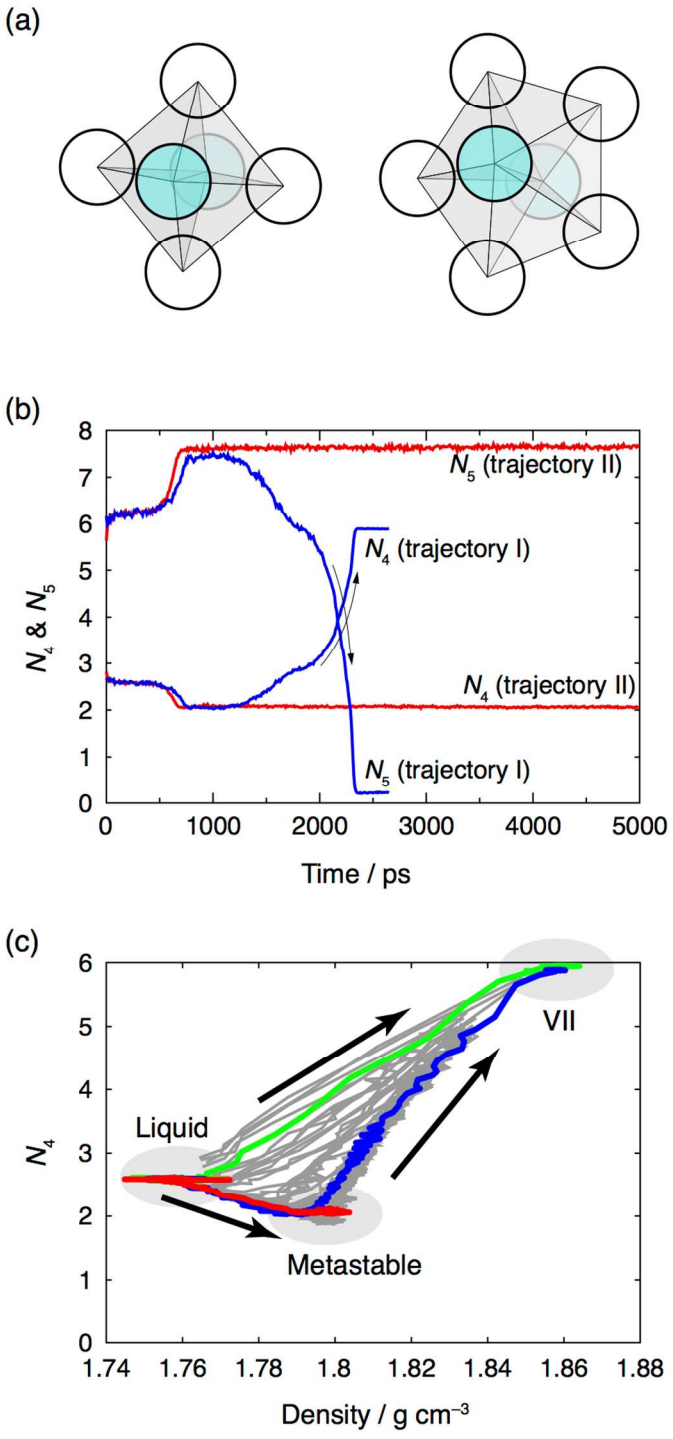

Figure 3. (a) Illustrations of the packings of spheres in tetragonal and pentagonal bipyramids. The light blue sphere indicates the apex of the pyramid. (b) Time evolution of the number of tetragonal bipyramids per water molecule (N_4) and pentagonal bipyramids per water molecule (N_5) in trajectories I and II. (c) All obtained trajectories projected to the number of tetragonal bipyramids per water molecule (N_4) and to density. Trajectories I, II, and III are colored in blue, red, and green, respectively.

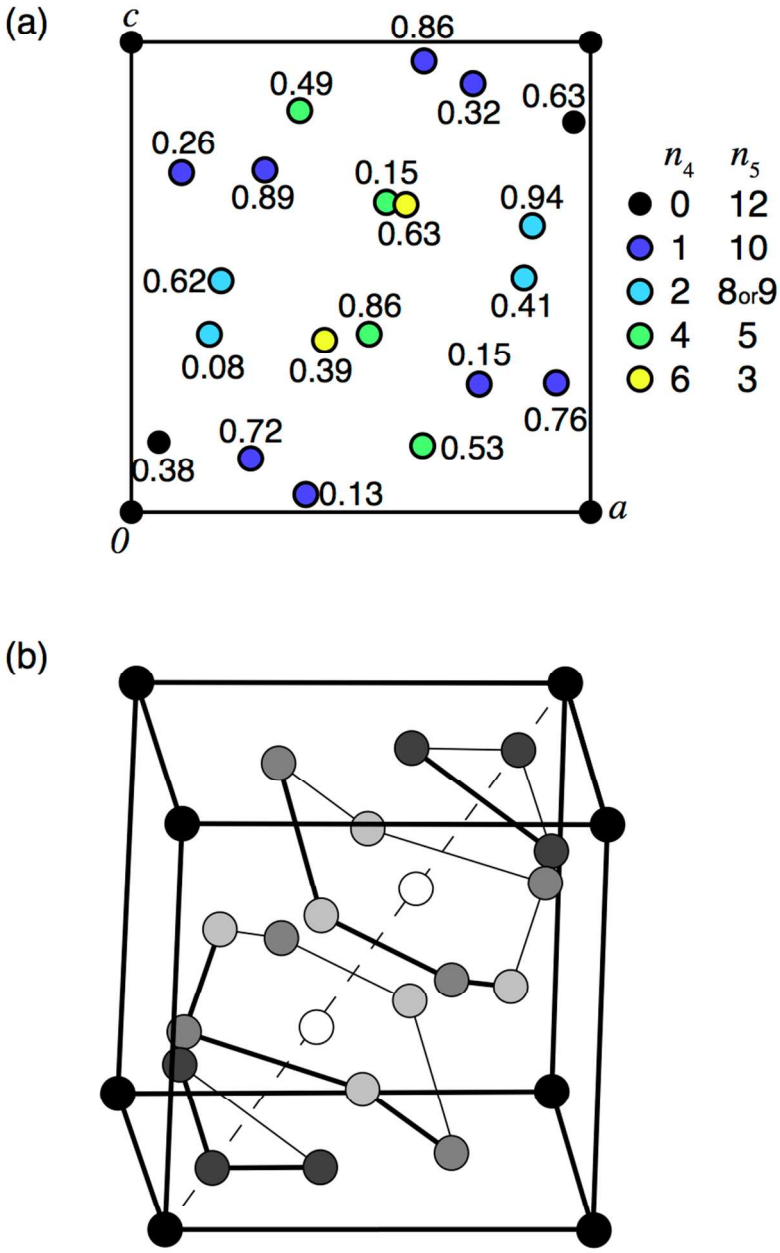

Figure 4. (a) An average structure of the unit cell estimated by pattern matching. It is projected to the ac plane. A circle represents the position of a water molecule. Numbers indicate the relative depth along axis b. Colors indicate n_4 and n_5, which are the number of tetragonal and pentagonal bipyramids that contain the site as the apex. (b) Ideal molecular positions in the rhombohedral unit cell. Lines are drawn to serve as a visual guide.

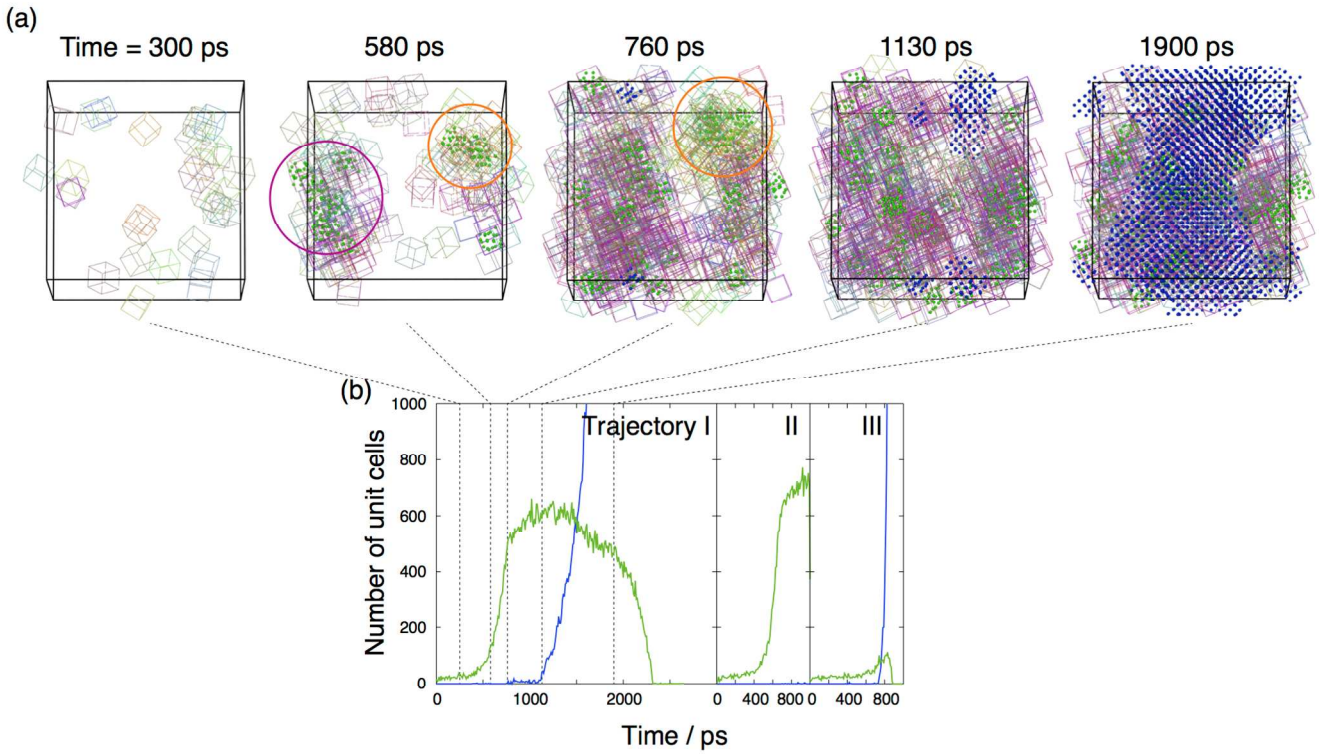

Figure 5. (a) Snapshots at 300 ps, 580 ps, 760 ps, 1130 ps, and 1900 ps in trajectory I. The cube represents the local structure loosely matched to a unit cell of the metastable phase (s < 10.0 Å^2). A similar color is assigned for the unit cells with a similar orientation. Green and blue dots represent the molecules strictly matched to a unit cell of the metastable phase and an eightfold unit cell of ice VII (s < 2.0 Å^2), respectively. Two different nuclei are indicated by purple and orange circles. (b) The total number of local structures that loosely matched with a unit cell of the metastable phase (green line) and strictly matched with an eightfold unit cell of ice VII (blue line), are represented by cubes and blue dots in Fig. 5(a), respectively. Note that the template may match the same molecule multiple times and therefore the number of unit cells is only a rough estimate of the size of the crystal nucleus.

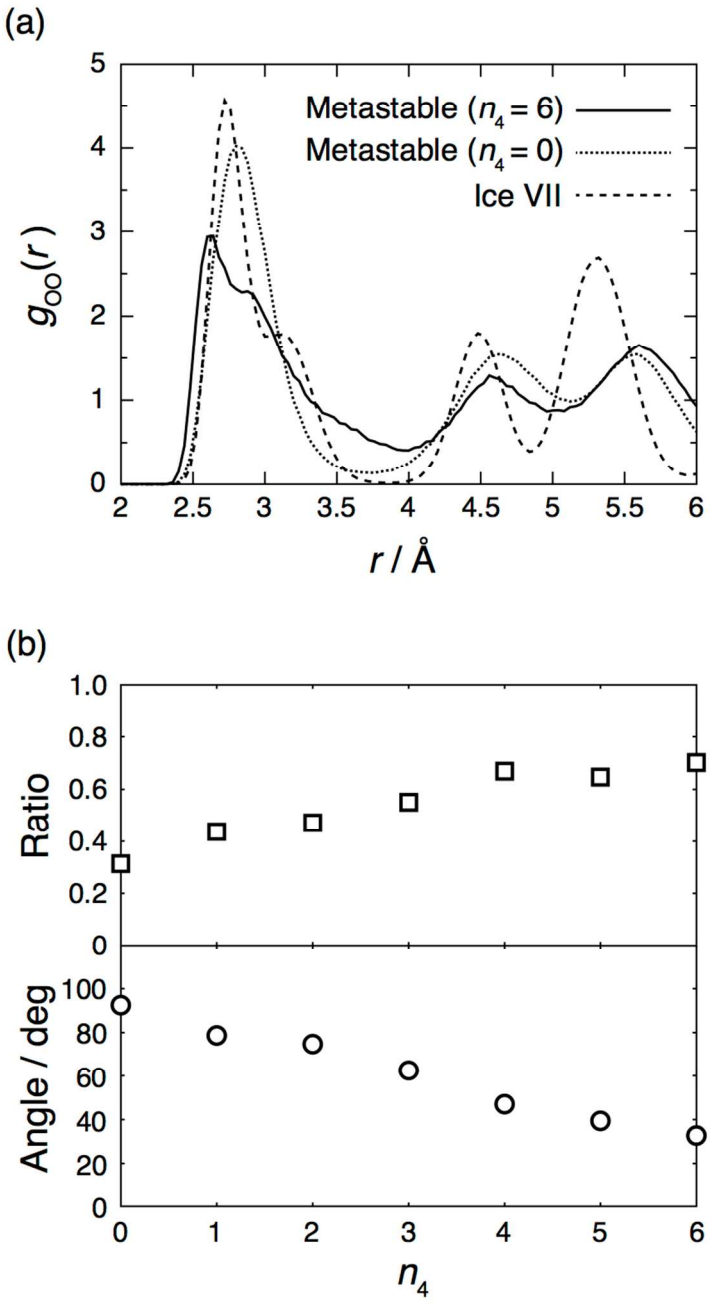

Figure 6. (a) Oxygen-oxygen RDFs, $g_{OO}(r)$. RDFs around the molecule with n_4=6 and n_4=0 in the metastable phase and all molecules in ice VII are plotted with solid, dotted, and dashed lines, respectively. (b) The ratio of water molecules having four hydrogen bonds and the average rotation angle within 10 ps plotted against n_4.